2022 IEEE 19th International Symposium on Biomedical Imaging (ISBI) | 978-1-6654-2923-8/22/$31.00 ©2022 IEEE | DOI: 10.1109/ISBI52829.2022.9761689

# QUANTIFYING NEWLY APPEARING REPLICATION FOCI IN CELL NUCLEI BASED ON 3D NON-RIGID REGISTRATION

*Qi Gao*[1]*, Vadim O. Chagin*[2,3]*, M. Cristina Cardoso*[3]*, and Karl Rohr*[1]

[1]Biomedical Computer Vision Group, BioQuant, IPMB, Heidelberg University and DKFZ, Germany
[2]Institute of Cytology, Russian Academy of Sciences, St. Petersburg, Russia
[3]Cell Biology and Epigenetics, Department of Biology, Technical University of Darmstadt, Germany

## ABSTRACT

Studying the dynamics of replication foci (RFi) in live cell microscopy images is important to understand the principles of DNA replication during the cell cycle. Whether new RFi appear in proximity to existing ones or randomly remains unclear. We propose two new methods to quantify newly appearing RFi which represent global and local spatial information. One method is based on proportion curves and a proximity score, and the second method is based on proximity distribution maps. In addition, to align the 3D temporal microscopy image sequences and improve quantification, we introduce a 3D elasticity model-based image registration method. Experiments using synthetic image data demonstrate the effectiveness of the proposed methods. We also show analysis results of appearing RFi in real confocal microscopy images.

***Index Terms*—** DNA replication foci, distribution estimation, non-rigid image registration, particle tracking

## 1. INTRODUCTION

Genomic DNA of eukaryotic cells is duplicated during the S-phase of the cell cycle in sites of active DNA replication that are spatially clustered in the nucleus. These distinct clusters, termed replication foci (RFi), can be visualized in microscopy images due to gathered proliferating cell nuclear antigen (PCNA) (see Fig. 1). In conventional wide-field and confocal microscopy, RFi generally correspond to replication domains (RDs) that consist of multiple replicons synchronously initiating DNA replication [1]. Recent studies based on super-resolution microscopy (*e.g.*, 3D-SIM, STORM) show that RFi may correspond to single replicons or even single replication forks [2, 3].

To better understand DNA replication, different properties of RFi such as number, size, distribution, lifetime, movement, and propagation have been studied (*e.g.*, [2, 4, 3, 5]). In the early S-phase, the number of RFi increases rapidly [6] to ensure their parallel activity as well as efficient and timely duplication of the whole genome. Important questions are: Do new RFi appear in proximity to existing ones or randomly? Are there regions where RFi appear more often? However, answering these questions is challenging. First, using only the Euclidean distances between RFi does not allow determining whether new RFi appear non-randomly or randomly. Second, RFi can move, fuse and resegregate [7]. Third, cell nuclei also move and undergo significant deformation (*cf*. Fig. 1). To the best of our knowledge, the two questions mentioned above have not been addressed quantitatively and in a general manner in previous work. Most closely related is the work in [5], where colocalization analysis was used to study the propagation pattern of RFi (*i.e.*, whether and how RFi overlap at different time points at a sub-RD level) and only global translation of image frames was corrected using cross-correlation. However, the proximity of newly appearing RFi w.r.t. existing ones was not analyzed.

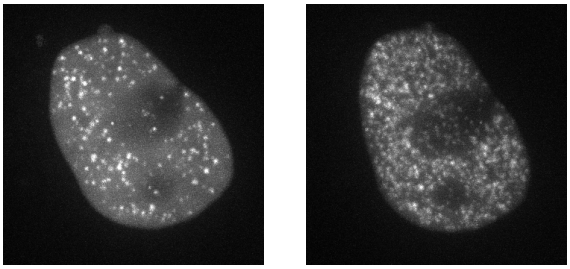

**Fig. 1**. 1st (left) and 6th frame (right) from a real image sequence of the nucleus of a HeLa cell entering the S-phase (maximum intensity z-projection). Note the intensity changes of RFi (bright spots) and the nucleus deformation.

To accurately quantify the proximity of newly appearing RFi w.r.t. existing ones as well as to distinguish these two types of RFi and estimate their distributions, non-rigid registration of cell nuclei in all frames of a temporal image sequence is needed. However, due to appearing RFi structures, common intensity-based non-rigid registration methods (*e.g.*, [8, 9]) generally do not perform well. If RFi structures are excluded for registration, the reduced intensity information is not sufficient to obtain good results. Thus, elasticity-based registration approaches (*e.g.*, [10, 11]) that rely on a strong deformation model, are preferable. However, these methods can only deal with 2D images.

In this paper, we propose two new methods to quantify

the proximity of appearing RFi to existing ones in 3D temporal microscopy image sequences. One method represents the global spatial information and we define a proximity score based on proportion curves. The other method represents local spatial information by proximity distribution maps. In addition, to cope with the movement and deformation of cell nuclei, we introduce a non-rigid registration method based on an elasticity model for 3D microscopy images. Our approach is general and can be used for images where RFi correspond to RDs or sub-RD structures (*e.g.*, single replicons). Experiments using synthetic images demonstrate the effectiveness of the proposed methods. We also show analysis results of appearing RFi in a real confocal microscopy image sequence.

## 2. METHODS

We describe two new methods to quantify newly appearing RFi: One is based on proportion curves and a proximity score, and the other is based on proximity distribution maps. Then, we introduce a non-rigid registration method for 3D cell images and a computational scheme to analyze appearing RFi in time-lapse microscopy images.

### 2.1. Quantification of newly appearing points

A natural way to evaluate the proximity of new RFi to existing ones is to directly check the Euclidean distances between them. However, since randomly appearing RFi may also be close to existing ones, using only the Euclidean distances does not allow determining whether new RFi appear non-randomly or randomly. Thus, the number and distribution of existing RFi must be taken into account.

**Proportion curves and proximity score.** We exploit two curves to visualize the proximity and randomness of new points (in our case RFi) appearing w.r.t. existing ones. The first curve is the proportion of the covered area (or volume) by circular (or spherical) neighborhoods of existing points with radius $r$ to the whole area (or volume), denoted by $l_{\mathrm{a}}(r)$, where $r \in [0, r_{\mathrm{min}}]$ and $r_{\mathrm{min}}$ is the minimal value satisfying $l_{\mathrm{a}}(r_{\mathrm{min}}) = 1$. The second curve is the proportion of new points appearing in circular (or spherical) neighborhoods of existing ones with radius $r$ to all new points, denoted by $l_{\mathrm{p}}(r)$, $r \in [0, r_{\mathrm{min}}]$. As illustrated in Fig. 2, when $l_{\mathrm{p}}(r)$ is located to the left of $l_{\mathrm{a}}(r)$, new points appear mostly or partially in proximity to existing ones; when the two curves roughly overlap, new points appear spatially randomly; $l_{\mathrm{p}}(r)$ located to the right of $l_{\mathrm{a}}(r)$ implies anti-proximity, meaning that new points tend to appear far away from existing ones. To quantify the degree of proximity or randomness, we define a proximity score

$$\rho = \frac{A_{\mathrm{p}}}{A_1} - \frac{A_{\mathrm{a}}}{A_2}, \tag{1}$$

where $A_{\mathrm{p}}$ is the area of regions between the curves with $l_{\mathrm{p}}(r) > l_{\mathrm{a}}(r)$, $A_{\mathrm{a}}$ is analogously defined with $l_{\mathrm{a}}(r) > l_{\mathrm{p}}(r)$, $A_2$ is the area under the $l_{\mathrm{a}}(r)$ curve, and $A_1 = r_{\mathrm{min}} - A_2$.

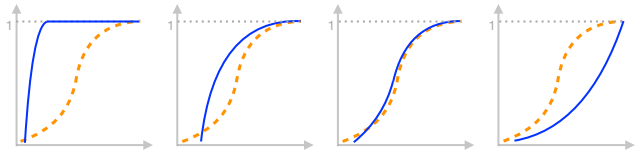

(a) $\rho > 0$ (b) $\rho > 0$ (c) $\rho \approx 0$ (d) $\rho < 0$

**Fig. 2**. Illustration of proportion curves and corresponding proximity score $\rho$ which provide global information about the pattern of newly appearing points w.r.t. existing ones: *(a)* mostly in proximity, *(b)* partially in proximity, *(c)* roughly random, *(d)* anti-proximity. Orange, dashed: proportion of covered area (or volume) by the neighborhoods of existing points to the whole area (or volume). Blue, solid: proportion of new points appearing in the neighborhood of existing points to all new points.

The value of $\rho$ lies in the range $[-1, 1]$, with $1$ and $-1$ indicating perfect proximity and anti-proximity, respectively, and $0$ indicating complete randomness. Since all points in the considered region are used to generate the proportion curves and to compute the proximity score, this method represents the *global* spatial statistics.

**Proximity distribution map.** As an alternative to the method above, we suggest a method based on a proximity distribution map. The distributions of existing points and new points in an image frame are computed using kernel density estimation (KDE). For better comparison between different frames, the computed distributions are normalized by the point number in a frame. Element-wise product of the two normalized distributions yields the proximity distribution map which provides *local* spatial information where newly appearing points occur more often in close proximity to existing points.

### 2.2. 3D non-rigid registration of cell nuclei

To quantify newly appearing RFi in 3D time-lapse microscopy image sequences using the proposed proximity quantification methods described above, non-rigid registration of cell nuclei is necessary. We extend the 2D registration method with elasticity constraints in [11] to cope with the considered 3D microscopy images. RFi structures are excluded for estimating the deformation. However, a direct extension by following [9] yielded unsatisfactory results. Major reasons include strongly different resolution in x- and y-direction compared to the z-direction (*e.g.*, factor of 5), much fewer slices compared to image height and width (resulting in difficulties of using a coarse-to-fine strategy), large deformation along the z-axis, and reduced intensity information due to excluding RFi for estimating the deformation.

To address the issues, we extend the previous method [11]. First, we use different weights in the regularization term of the deformation model for the partial derivatives in z-direction than in x- and y-direction according to the difference in resolution. Second, we employ a special 3D image pyramid for

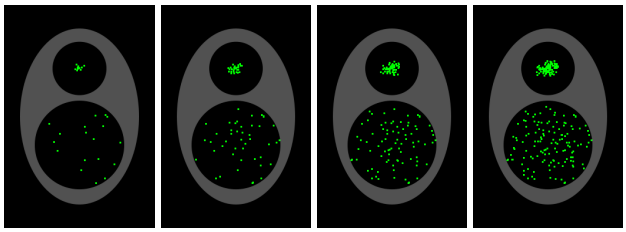

(a) 3rd frame (b) 5th frame (c) 7th frame (d) 9th frame

**Fig. 3**. Frames (maximum intensity projection) of synthetic 3D image sequence.

the coarse-to-fine strategy to handle large deformations. We use multiple scales for the x- and y-direction, but only one scale for the z-direction; and use a varying weight for each pyramid scale. Third, we perform an affine pre-registration.

### 2.3. Analysis of appearing RFi in microscopy images

To analyze appearing RFi in time-lapse microscopy images of cell nuclei using the proposed proximity quantification methods, we developed a computational scheme consisting of (i) non-rigid registration of cell nuclei, (ii) RFi detection and association, and (iii) proximity quantification of RFi.

Non-rigid registration is performed using the method described in Sec. 2.2. RFi are detected using a spot detector in the original (unregistered) image frames and then their coordinates are transformed using the deformation fields determined by non-rigid registration. A global nearest-neighbor association (using the Hungarian algorithm) of the RFi coordinates is used to distinguish existing RFi and newly appearing RFi in each frame. With the (transformed) coordinates of existing and newly appearing RFi, the proposed proximity quantification described in Sec. 2.1 is then performed.

## 3. EXPERIMENTS

**Data.** We use both synthetic and real time-lapse microscopy images to evaluate the proposed methods. We generate a synthetic 3D image sequence with 9 frames of $380 \times 255 \times 255$ voxels including 224 points distributed in two sub-regions. In the upper region, new points appear in close proximity (3- or 4-voxel Chebyshev distance) to existing ones, while in the lower region, new points appear randomly (Fig. 3). The real 3D time-lapse image sequence includes 10 frames of $350 \times 350 \times 27$ voxels generated by a confocal microscope with a resolution of $104\text{nm} \times 104\text{nm} \times 500\text{nm}$, showing RFi (expressed by fluorescently tagged PCNA) in nuclei of HeLa cells during S-Phase [2] (Fig. 1).

### 3.1. Results on synthetic images

We used the 3D synthetic images to validate the proposed methods for proximity quantification, since point coordinates

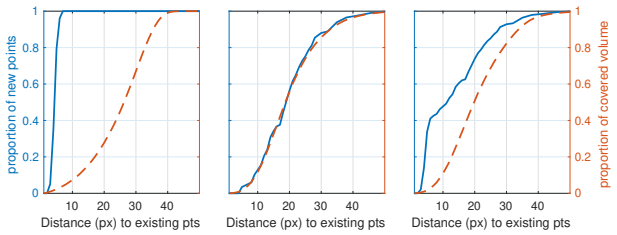


(a) Upper region, $\rho = 0.84$ (b) Lower region, $\rho = 0.02$ (c) All regions, $\rho = 0.36$

**Fig. 4**. Proportion curves and proximity scores of synthetic image sequence (4th to last frame).

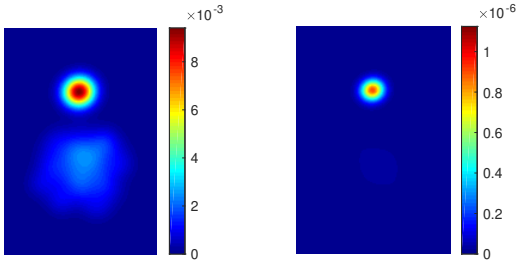


**Fig. 5**. Estimated distributions of synthetic image sequence (2D marginals of 3D distributions). *(Left)* Average (rescaled) point distribution. *(Right)* Average proximity distribution map of newly appearing points w.r.t. existing ones.

and the patterns of newly appearing points are known. Computed proportion curves and corresponding proximity scores are shown in Fig. 4. We considered the 4th frame to the last frame, since for the first three frames there are too few points to obtain robust results. As can be seen, the resulting proportion curves and proximity scores for the upper and lower region (non-random *vs*. random appearance) agree with the expectation (*cf*. Fig. 2). The proportion curves for the whole image in Fig. 4(c) show new points appear partially in close proximity to existing points. Thus we can answer the first question in Sec. 1.

For computing the proximity distribution maps, we used a Gaussian kernel ($\sigma = 16$) for the KDE. The average point distribution (Fig. 5(a), 2D marginal of the 3D distribution) indicates the regions where points appear more often. Thus we can answer the second question in Sec. 1. The average proximity distribution map (Fig. 5(b), also marginal distribution), obtained by computing the element-wise products of distributions of new points and existing ones, provides the spatial information where newly appearing points occur more often in close proximity to existing points.

### 3.2. Results on real microscopy images

To analyze the real 3D microscopy image sequence we registered the nuclei in all frames using the proposed 3D registration method (Sec. 2.2). To obtain an unbiased analysis result, RFi structures were excluded from deformation estimation by thresholding the image intensities. The registra-

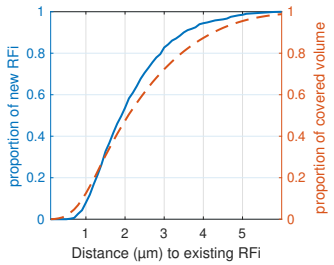


**Fig. 6**. Proportion curves with proximity score $\rho = 0.11$ of real confocal microscopy image sequence.

tion performance was quantified by the Dice scores between the nucleus in the reference frame (first frame) and that in all other frames, which were computed based on the segmentation of nuclei using a thresholding method with fixed parameters. For the unregistered images the average Dice score is $0.766$. The directly extended 3D method and the proposed 3D method achieved an average Dice score of $0.899$ and $0.942$, respectively. Thus, the proposed method yields a substantially improved result. RFi were detected using the 3D difference-of-Gaussians (DoG) filter, and associations were determined by a nearest neighbor approach (radius of $1.5$ µm). For the KDE, a Gaussian kernel with $\sigma = 1.6$ µm was employed.

The proportion curves and the proximity score $\rho = 0.11$ (Fig. 6) suggest that, inside the nucleus, new RFi appear not completely randomly, but partially in proximity to existing RFi. There is some tendency for new RFi to appear about $1 \sim 2$ µm away from existing RFi (according to the steepest part of the curve, see Fig. 6). The distributions of the RFi inside the nucleus and the proximity distribution map of new RFi w.r.t. existing ones are shown in Fig. 7 (see Supplementary Movie 1 for the proximity distribution map in 3D). It can be seen that, in some sub-regions inside the nucleus, newly appearing RFi occur somewhat more often in proximity to existing ones.

## 4. SUMMARY

We proposed new methods for quantifying the proximity of newly appearing RFi w.r.t. existing ones. The proposed methods are general and can also be used for appearance analysis of other spot-like structures. To accurately distinguish new RFi from existing ones within cell nuclei undergoing significant deformation, we introduced an elasticity model-based registration method for 3D temporal microscopy images. We applied our methods to synthetic data and real time-lapse image sequences of cell nuclei. The experiments show the effectiveness of the proposed methods which provide global and local proximity information of appearing RFi.

**Acknowledgments.** Support of the DFG within the SPP 2202 (RO 2471/10-1, CA 198/15-1) and the BMBF project de.NBI (031A537C, HD-HuB) is gratefully acknowledged.

**Compliance with ethical standards.** This work is a study for which no ethical approval was required.

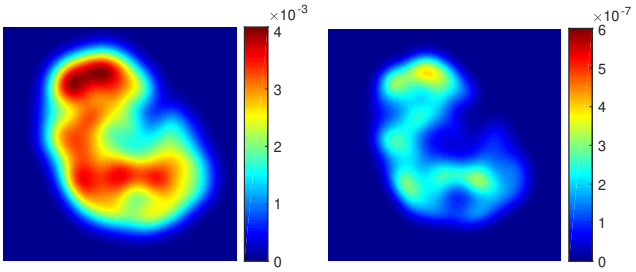

**Fig. 7**. Estimated distributions of real microscopy image sequence (2D marginals of 3D distributions). *(Left)* Average (rescaled) RFi distribution. *(Right)* Average proximity distribution map of newly appearing RFi w.r.t. existing ones.

## 5. REFERENCES

[1] C. Marchal, J. Sima, and D. M. Gilbert, "Control of DNA replication timing in the 3D genome," *Nat. Rev. Mol. Cell Biol.*, vol. 20, pp. 721–737, 2019.

[2] V. O. Chagin, C. S. Casas-Delucchi *et al.*, "4D visualization of replication foci in mammalian cells corresponding to individual replicons," *Nat. Commun.*, vol. 7, no. 11231, 2016.

[3] W. Xiang, M. J. Roberti, J. Heriche, S. Huet, S. Alexander, and J. Ellenberg, "Correlative live and super-resolution imaging reveals the dynamic structure of replication domains," *J. Cell Biol.*, vol. 217, no. 6, pp. 1973–1984, 2018.

[4] P. J. M. Zessin, A. Sporbert, and M. Heilemann, "PCNA appears in two populations of slow and fast diffusion with a constant ratio throughout S-phase in replicating mammalian cells," *Scientific Reports*, vol. 6, no. 18779, 2016.

[5] Q. P. Su, Z. W. Zhao *et al.*, "Superresolution imaging reveals spatiotemporal propagation of human replication foci mediated by CTCF-organized chromatin structures," *Proc. Natl. Acad. Sci. U. S. A.*, vol. 117, no. 26, pp. 15 036–15 046, 2020.

[6] D. Löb, N. Lengert, V. Chagin *et al.*, "3D replicon distributions arise from stochastic initiation and domino-like DNA replication progression," *Nat. Commun.*, vol. 7, no. 11207, 2016.

[7] P. Meister, A. Taddei *et al.*, "Replication foci dynamics: replication patterns are modulated by S-phase checkpoint kinases in fission yeast," *The EMBO Journal*, vol. 26, no. 5, 2007.

[8] M. Tektonidis and K. Rohr, "Diffeomorphic multi-frame non-rigid registration of cell nuclei in 2D and 3D live cell images," *IEEE Trans. Image Process.*, vol. 26, no. 3, pp. 1405–1417, 2017.

[9] Q. Gao and K. Rohr, "A global method for non-rigid registration of cell nuclei in live cell time-lapse images," *IEEE Trans. Med. Imag.*, vol. 38, no. 10, pp. 2259–2270, 2019.

[10] D. V. Sorokin, I. Peterlik *et al.*, "Non-rigid contour-based registration of cell nuclei in 2-D live cell microscopy images using a dynamic elasticity model," *IEEE Trans. Med. Imag.*, vol. 37, no. 1, pp. 173–184, 2018.

[11] Q. Gao, V. O. Chagin, M. C. Cardoso, and K. Rohr, "Non-rigid registration of live cell nuclei using global optical flow with elasticity constraints," in *Proc. IEEE Int. Symp. on Biomed. Imag.*, 2021, pp. 1457–1460.